Ultrahigh-Field ^{25}Mg NMR and DFT Study of Magnesium Borate Minerals

Bing Zhou,[1][§] Alexandra Faucher,[2][†][§] Robert Laskowski,[3] Victor V. Terskikh,[4] Scott Kroeker,[5] Wei Sun,[6,7] Jinru Lin,[6] Jin-Xiao Mi,[7] Vladimir K. Michaelis[2*] and Yuanming Pan[6*]

1. College of Materials Science and Engineering, Tongji University, Shanghai 21000, China

2. Department of Chemistry, University of Alberta, Edmonton, Alberta T6G 2G2, Canada

3. Institute of High Performance Computing, A*STAR, 1 Fusionopolis Way, #16-16, Connexis, Singapore 138632

4. Department of Chemistry, University of Ottawa, Ottawa, Ontario K1N 6N5 Canada

5. Department of Chemistry, University of Manitoba, Winnipeg, Manitoba R3T 2N2, Canada

6. Department of Geological Sciences, University of Saskatchewan, Saskatoon, Saskatchewan S7N 5E2, Canada

7. Fujian Provincial Key Laboratory of Advanced Materials, Department of Materials Science and Engineering, College of Materials, Xiamen University, Xiamen 361005, Fujian Province, China

[†]Current address: Bernal Institute, University of Limerick, Limerick, Republic of Ireland

[§]BZ and AF contributed equally

*Corresponding authors: Vladimir K. Michaelis (vladimir.michaelis@ualberta.ca) and Yuanming Pan (yuanming.pan@usask.ca)

Keywords: MAS NMR, grandidierite, quantum chemical calculations, WURST, CPMG, wideline, NMR crystallography

ABSTRACT

A series of well-characterized magnesium borate minerals and synthetic analogues have been studied via ultrahigh-field ^{25}Mg solid-state nuclear magnetic resonance (NMR) spectroscopy. Correlations between ^{25}Mg NMR parameters and the local structure at the magnesium site(s) are highlighted and discussed. First-principles density functional theory calculations of ^{25}Mg NMR parameters carried out with the WIEN2k software package support our experimental ^{25}Mg NMR data. Experimental ^{25}Mg C_Q values range from 0.7 ± 0.1 MHz in hungchaoite to 18.0 ± 0.5 MHz in boracite-type $Mg_3B_7O_{13}Br$. The latter C_Q value is, to our knowledge, the largest reported ^{25}Mg nuclear quadrupole coupling constant in the literature to date. In general, C_Q values correlate positively with the degree of geometrical distortion at the Mg site, despite the diversity in nearest-neighbor ligands (O^{2-}, OH^-, H_2O, F^-, Cl^- and Br^-) across the series of magnesium borates. Experimental δ_{iso} values range from 0.2 ± 0.5 ppm in hungchaoite to 23 ± 3 ppm in grandidierite, which are within the expected chemical shift range for diamagnetic magnesium borates.

1 INTRODUCTION

Magnesium is the second most abundant element by mole-fraction and the third most abundant element by mass in the Earth,[1] and ranks as the third most abundant element dissolved in seawater, after Na and Cl. Magnesium, as a strongly lithophilic element, combines readily with oxygen to form diverse minerals (e.g., borates, carbonates, oxides/hydroxides, silicates and sulfates) on Earth's surface. For example, magnesium borates are common minerals in salt spring deposits and evaporites, and are known to feature great structural diversity arising from the complex linkages of $^{[3]}BO_3$ and $^{[4]}BO_4$ groups and from the presence of different Mg coordination environments.[2-9]

Magnesium has three stable isotopes, ^{24}Mg, ^{25}Mg and ^{26}Mg; however, only ^{25}Mg, which has a non-zero nuclear spin quantum number, $I = 5/2$, is amenable to study *via* solid-state nuclear magnetic resonance (NMR) spectroscopy. One significant challenge encountered when utilizing ^{25}Mg NMR spectroscopy as a structural tool is the experimental difficulty arising from several unfavorable NMR properties of this isotope. For example, ^{25}Mg has a small gyromagnetic ratio, $\gamma = -1.639 \times 10^7$ rad·s^{-1}·T^{-1}, a moderate nuclear electric quadrupole moment, $Q = 19.94$ fm^2, and a relatively low natural abundance of 10%, resulting in sensitivity that is approximately four orders of magnitude less than that for ^1H.[10] These experimental difficulties have historically hampered the application of ^{25}Mg NMR spectroscopy to solving problems in chemistry and geology.[11-14]

Recent advances in ^{25}Mg NMR spectroscopy stem largely from the availability of ultrahigh-field magnets, i.e., $B_0 \geq 18.7$ T, that increase the NMR sensitivity and enhance the resolution for NMR spectra of quadrupolar nuclei of samples under both non-spinning and magic-angle spinning (MAS) conditions. As well, ^{25}Mg NMR spectroscopy has benefitted from the development of sensitivity-enhancement techniques and multiple-echo acquisition methods for quadrupolar nuclei.[11, 15-17] These technical advances have allowed the collection of ^{25}Mg NMR spectra with sufficient signal-to-noise (S/N) ratio and resolution to identify distinct Mg environments in solids.

Experimental ^{25}Mg MAS NMR parameters in various solids have been shown to be sensitive to the structural environment at magnesium.[12, 18, 19] Two parameters, longitudinal strain, $|\alpha|$, and shear strain, $|\psi|$, introduced by Ghose and Tsang (1973),[20] can be used to quantify the distortion of coordination polyhedra, i.e., describe the local structure at the observed nucleus. For several nuclei, e.g., ^{11}B, ^{23}Na, ^{27}Al and ^{73}Ge, correlations between nuclear quadrupole coupling constants, C_Q, and $|\alpha|$ or $|\psi|$ have been documented,[21-25] suggesting that effects from the local chemical environment dominate the electric field gradient (EFG) at the observed nucleus. To date, empirical correlations between ^{25}Mg NMR parameters and the Mg local structural environments have been documented for several families of Mg compounds such as phosphates, aluminates, oxides, silicates, sulfates, nitrates, and carboxylates.[11, 12, 16, 17, 19] However, there have been relatively few ^{25}Mg NMR studies of borates.[7, 26] Borates are known to feature diverse Mg coordination polyhedra with a wide variety of nearest-neighbor ligands (O^{2-}, OH^-, H_2O, F^-, Cl^- and Br^-), including unusual structures such as the extremely elongated [MgO_4Br_2] tetragonal dipyramid with Mg-Br and Mg-O bond lengths of 3.009 and 2.015 Å, respectively, in cubic $Mg_3B_7O_{13}Br$;[9] and the highly asymmetrical [MgO_4Cl] and [MgO_5] polyhedra in boracite ($Mg_3B_7O_{13}Cl$) and MgB_4O_7, respectively.[2, 27, 28]

These peculiarities in the magnesium environment motivated us to investigate a suite of well-characterized magnesium borate minerals and synthetic analogues with diverse local structural environments by ^{25}Mg NMR spectroscopy at ultrahigh magnetic field strength (B_0 = 21.1 T). Analysis of the ultrahigh-field ^{25}Mg NMR spectra obtained in this study provide chemical shift and quadrupolar parameters, which are supported by periodic first-principles calculations implementing an all electron approach within the WIEN2k software package. The experimental and theoretical data are used collectively to establish relationships between ^{25}Mg NMR parameters and local chemical structure, providing insight into the chemistry of magnesium borate minerals.

2 THEORETICAL BACKGROUND

2.1 Solid-state nuclear magnetic resonance parameters

Magnesium-25 is a quadrupolar nucleus, i.e., it has a non-spherical charge distribution, which leads to coupling between the nuclear electric quadrupole moment, Q, and the local electric field gradient. The quadrupolar interaction is described by two parameters, the nuclear quadrupole coupling constant, C_Q (Equation 1), and the asymmetry parameter, η (Equation 2).

$$C_Q = eQV_{zz}/h \qquad\qquad (1)$$

$$\eta = (V_{xx} - V_{yy})/V_{zz} \qquad\qquad (2)$$

Here, e is the charge of an electron, Q is the nuclear electric quadrupole moment intrinsic to the nucleus of interest, h is Planck's constant and V_{mm} (m = x, y, z) are eigenvalues of the electric field gradient (EFG), defined such that $|V_{xx}| \leq |V_{yy}| \leq |V_{zz}|$. When the magnitude of the quadrupolar interaction is non-zero, the NMR lineshape of a quadrupolar nucleus possesses characteristic features and broadening; the values of both C_Q and η impact the NMR line width, while the quadrupolar NMR lineshape is described by η. Of relevance to this research, the central transition ($m_I = 1/2 \leftrightarrow -1/2$) will be broadened if $|C_Q|$ is large enough; here, the quadrupolar interaction can be described as a perturbation to the Zeeman interaction in which the 2nd order term is considered. Further theoretical details can be found within the references listed.[29-31]

Chemical shift anisotropy (CSA) may also influence the spectral appearance of solids. In this research we report chemical shift tensors using the Herzfeld-Berger method,[32, 33] the average, or isotropic ^{25}Mg chemical shift is given by

$$\delta_{iso} = (\delta_{11} + \delta_{22} + \delta_{33}) / 3 \qquad (3)$$

where the values δ_{nn} (n = 1, 2, 3) describe the symmetric part of the chemical shift interaction tensor. The overall breadth of the CSA NMR powder pattern is given by the span, Ω (Equation 4), while the shape of the NMR powder pattern is described by the skew, κ (Equation 5).

$$\Omega = \delta_{11} - \delta_{33} \qquad (4)$$

$$\kappa = 3(\delta_{22} - \delta_{iso}) / \Omega \qquad (5)$$

2.2 Quantum Chemical Calculations

The DFT-based approach for periodic solids, PAW and GIPAW,[34, 35] which employ the plane-wave pseudopotential formalism, have been used for the calculations of EFG and magnetic shielding parameters for a wide range of inorganic crystalline systems including Mg compounds.[12, 16, 18] However, Charpentier (2011)[34] noted that the use of the plane-wave expansion smears localized features (in contrast to the use of localized basis sets), which could mask contributions to the magnetic shielding. Thus, the ultra-soft pseudo-potential describing the interactions between core and valence electrons for the GIPAW modeling implemented within the CASTEP software[36-38] may lead to unphysical behavior and thus misleading conclusions.[34] As an alternative approach for periodic solids, this work utilizes the full-potential linearized augmented plane wave (FP-LAPW) method as implemented within the WIEN2k software.[39-48] The FP-LAPW formalism, which in principle does not impose any simplification or approximation to the core and valence states, allowing for core relaxation, is a more accurate representation of the electronic environment but computationally more costly compared to the pseudo-potential approach.

The structural model built from X-ray diffraction results underwent a geometrical optimization prior to carrying out NMR calculations. In our previous borate studies[8, 9, 26, 49, 50] this approach was necessary to improve the calculated results because it is difficult to accurately locate the positions of light elements such as H, B, and F, *via* X-ray diffraction.[8, 26, 49] As such, a comparison of the

6

theoretically calculated NMR parameters (chemical shielding and EFG tensors) with the experimentally measured NMR parameters (δ_{iso}, C_Q, η) may provide refinements of the structural models obtained via diffraction methods.

3 EXPERIMENTAL

3.1 Materials and Characterization

Samples of magnesium borate minerals including fluoborite (Bodar Quarry, New Jersey, USA); grandidierite (Andrahomana, Madagascar); hungchaoite (Tibet, China); szaibelyite (Kazakhstan); sinhalite (Sri Lanka); inderite and kurnakovite (Boron, California, USA) were visually inspected, to select transparent crystallites to minimize the inclusions of transition metal impurities. The synthetic series studied includes boracite, cubic-$Mg_3B_7O_{13}Br$, MgB_4O_7, kotoite, and suanite. Boracite and cubic-$Mg_3B_7O_{13}Br$ samples were synthesized via the boric acid flux method.[9] Briefly, for the sample of boracite this involved heating 1 g of $MgCl_2$ between two 0.5 g layers of H_3BO_3 in a Teflon-lined stainless steel autoclave at 240 °C for 72 hrs; for the $Mg_3B_7O_{13}Br$ sample, 0.3 g of $MgBr_2$ and 0.5 g B_2O_3 were heated to 500 °C in an evacuated silica tube for 72 hrs. Synthesis of MgB_4O_7 involved heating a $MgO:B_2O_3$ mixture at the molar ratio of 1:3 in a platinum crucible at 750 °C and atmospheric pressure for 24 hrs. Kotoite and suanite were synthesized by dissolving $MgCl_2 \cdot 6H_2O$ and H_3BO_3 in deionized water at stoichiometric proportions (3:2 for kotoite and 1:1 for suanite), followed by heating of the solutions to 110 °C until the stoichiometric gel products formed by evaporation (~24 hrs). Gels were then transferred to platinum crucibles and maintained at 700 °C for 2 days.

All samples were ground into a fine powder using an agate mortar and pestle before characterization via powder X-ray diffraction (XRD). Powder XRD was performed using either a PANalytical X'pert PRO X-ray diffractometer using Co $K_{\alpha1}$ radiation (λ = 1.78895 Å) at 40 kV and

45 mA, or on an Intel MPD multi-purpose diffractometer system using Cu K_α radiation ($\lambda = 1.54056$ Å) at 40.1 kV and 20 mA. Powder XRD results (Figures S1-S7) show that most samples are highly crystalline and highly pure (> 99%), exceptions include synthetic kotoite and MgB_4O_7 where minor impurities (< 5 %) of MgO are observed (Figures S1 and S4).

3.2 *Solid-State NMR Spectroscopy*

Magnesium-25 NMR spectra were acquired on a Bruker Avance II NMR spectrometer with B_0 = 21.1 T ($v_0(^1H)$ = 900 MHz, $v_0(^{25}Mg)$ = 55 MHz) at the National Ultrahigh-Field NMR Facility for Solids (National Research Council Canada, Ottawa, Canada). NMR spectra were collected using either a 4 mm double channel (H-X) MAS NMR Bruker probe or single-channel 5 (or 7) mm home-built probes. The MAS rotor frequency was set to 16.5 kHz for all MAS NMR spectra except for those acquired for the hungchaoite, suanite, and szaibelyite samples, for which the rotor frequencies were 10, 10, and 18 kHz, respectively. The Bloch, Hahn echo, quadrupolar echo or WURST-CPMG[15, 51, 52] pulse sequences were used to collect the ^{25}Mg NMR spectra depending on the sample. All samples were acquired using magic-angle spinning except for MgB_4O_7, $Mg_3B_7O_{13}Cl$ and $Mg_3B_7O_{13}Br$. WURST pulses were 50 μs in length, and possessed a nominal bandwidth of 500 (MgB_4O_7 and $Mg_3B_7O_{13}Br$) or 750 kHz (boracite). Otherwise, a rectangular pulse was used to selectively excite the central transition ($m_I = 1/2 \leftrightarrow -1/2$). Selective pulses were determined *via* the relationship $PW_{90°}/(I + \frac{1}{2})$, where $PW_{90°}$ is the 90° pulse width determined using the reference solution. Recycle delays were checked for each sample to ensure sufficient relaxation; delays varied from 1 to 60 seconds. The spectral acquisition times ranged between 1 and 108 hrs, with most spectra requiring less than 24 hrs of spectrometer time to acquire. High-power continuous-wave proton decoupling (^1H v_{rf} = 50 kHz) was applied when acquiring ^{25}Mg NMR spectra of fluoborite, hungchaoite, and szaibelyite. Note that ^1H decoupling had no visible effect on the ^{25}Mg NMR

lineshape for fluoborite. All ^{25}Mg NMR spectra were acquired at natural abundance and referenced to 1 M aqueous $MgCl_2$ at δ_{iso} = 0 ppm. A complete summary of the ^{25}Mg NMR acquisition parameters is available in Table S1.

NMR spectra were processed using TOPSPIN, with 50 to 500 Hz exponential line broadening; where echo spectra were left-shifted as appropriate before Fourier transformation. NMR spectral simulations generated with WSolids[53] were used to determine the experimental ^{25}Mg NMR parameters. Uncertainties in ^{25}Mg NMR parameters were determined visually by comparing the simulated and experimental NMR spectra.

3.3 First-Principles Calculations

For the full-potential linearized augmented-planewave (FP LAPW) calculations using the WIEN2k software package, the following atomic-sphere radii (*RMT*), given in atomic units (a.u.), were used so that the calculations ran with the highest efficiency without any overlapping atomic spheres: H (0.65), B (1.3), O (1.6), Mg (1.89), Al (1.8), Cl (2.08) and Br (2.5). All calculations were based on the LAPW+lo method, with the core electron states separated from the valence states at −6.0 Ry. Calculations were performed at a plane-wave cut-off defined by min(*RMT*)*max(k_n) of 3.5, 7.0 for structures with and without hydrogen atoms in the unit cell, respectively; such a cut-off value corresponds to approximately 10,000 plane waves. Based on the variation of the total number of *k*-points in the Irreducible Brillouin Zone, 32 *k*-points were sufficient to achieve convergence for the final NMR (EFG and CSA) results. Angular momentum components up to *l* = 12 were included for the wave functions inside the atomic spheres. The self-consistent field (SCF) calculations were run in a non-spin polarized mode and the convergent condition for SCF was set at 2×10^{-5} eV. All of the above setups have been shown to be adequate for producing stable convergent results. The optimization employed the experimental XRD fractional atomic coordinates as the starting values and kept the unit cell parameters unchanged. Then, using a definition of the incremental interval,

the atomic coordinates were optimized by reducing the forces acting on each atom <2 mRy/a.u. The retention of the unit cell parameters from room-temperature XRD experiments *vs* a default thermal relaxation to 0 K, was intended to facilitate direct comparison with data obtained from room-temperature NMR spectra.[54] Calculations using the optimized structures of inderite and kurnakovite yielded significantly more accurate C_Q and η values than those calculated from the original XRD structures in our previous study,[26] hence results from this research were performed with XRD crystal structures[2-5, 9, 27, 55-62] which underwent a full optimization of atom positions while the unit cell parameters were kept constant. Calculations were performed on the Grex SGI Altix XE 1300 cluster, which consists of 316 compute nodes, each with two 6-core Intel Xeon X5650 2.66 GHz processors (Westgrid, Compute Canada, University of Manitoba).

Calculated ^{25}Mg isotropic magnetic shielding values, σ_{iso}, were converted to calculated ^{25}Mg isotropic chemical shift values, δ_{iso}, to facilitate comparison between experimental and calculated data. σ_{iso} is defined as $(\sigma_{xx} + \sigma_{yy} + \sigma_{zz})/3$, where σ_{xx}, σ_{yy}, and σ_{zz} are the principal components of the magnetic shielding tensor. When absolute shielding constants have not been determined, there are two common approaches for calculating δ_{iso} values from σ_{iso} values predicted using quantum chemistry calculations: (1) using a reference taken from an unconstrained (slope $\neq -1$) linear fit of the calculated absolute shieldings, or (2), scaling to the absolute magnetic shielding of a reference compound ($\delta_{iso} = -(\sigma_{iso} - \sigma_{ref})$). In this research, the experimental isotropic chemical shifts of three compounds, brucite ($Mg(OH)_2$), periclase (MgO), and spinel ($MgAl_2O_4$)[16, 63] were plotted against the corresponding DFT calculated isotropic magnetic shielding values (Figure S10). A linear regression analysis of these data gave a shielding reference value, σ_{ref}, of 564.5 ppm. Using this value, all calculated isotropic magnetic shielding values were converted to isotropic chemical shifts via the relationship $\delta_{iso} = -(\sigma_{iso} - 564.5 \text{ ppm})$.

4 RESULTS

4.1 Experimental and Calculated ^{25}Mg NMR Data

The magnesium borates in this research are subdivided into three categories based on the atom bonded to Mg, and are discussed in the following order; an anhydrous series consisting of kotoite, suanite, sinhalite, grandidierite and MgB_4O_7, a hydrous series consisting of szaibelyite, huangchaoite, inderite, kurnakovite, and hydroxylborite, and a halide series consisting of fluoborite, boracite and cubic $Mg_3B_7O_{13}Br$. Experimental and calculated ^{25}Mg NMR parameters, δ_{iso}, C_Q, and η, for all magnesium borates are reported in Table 1. Magnesium-25 NMR spectra of non-spinning samples possess lineshapes consistent with the quadrupolar interaction modeled as a perturbation to the Zeeman interaction to second order, which were broad compared to the relatively small chemical shift range of ^{25}Mg. Therefore, if present, anisotropy in chemical shift is expected to have negligible impact on the NMR lineshape. Simulations of ^{25}Mg NMR spectra did not include orientation-dependent contributions to the NMR lineshape due to anisotropy in chemical shift. Note that the sign of C_Q values cannot be determined from our experimental NMR data (the breadth of the NMR lineshape $\propto C_Q^2/v_o$) therefore the experimental C_Q values are reported as absolute values. Our quantum chemical calculations predict the signs of the quadrupolar coupling constants, which are reported in Table 1.

4.1.1 Anhydrous Series

Magnesium-25 MAS NMR spectra of kotoite, suanite, and grandidierite are shown in Figure 1a-c. The crystal structure of kotoite, which belongs to orthorhombic space group $Pnmn$,[56] contains two nonequivalent $[MgO_6]$ octahedra (1:2 ratio) in the unit cell. The ^{25}Mg MAS NMR spectrum of kotoite correspondingly has two distinct NMR powder patterns with lineshapes consistent with the quadrupolar interaction. In addition to the two NMR powder patterns, the ^{25}Mg NMR spectrum of

kotoite possesses a sharp resonance at *ca.* 26 ppm and corresponding spinning sidebands from MgO, an impurity in the sample. The quadrupolar coupling constants for kotoite are 6.85 and 3.75 ± 0.10 MHz for sites 1 and 2; δ_{iso} values for these two sites are 14 and 4 ± 2 ppm, respectively (Table 1). The experimental C_Q and δ_{iso} values for site 1 are based on our calculated C_Q and δ_{iso} values for this site as the signal-to-noise ratio of the broad ^{25}Mg NMR powder pattern was too low to afford definitive analysis.

Suanite crystallizes in monoclinic space group $P2_1/c$.[58] The unit cell contains two crystallographically nonequivalent Mg^{2+} sites in a 1:1 ratio, with each Mg atom coordinated by six oxygen atoms.[58] The ^{25}Mg MAS NMR spectrum reflects this, with two overlapping MAS NMR powder patterns corresponding to the two crystallographically nonequivalent magnesium sites (Figure 1b). Simulation of the ^{25}Mg NMR spectrum of suanite yielded $C_Q = 4.4 \pm 0.4$ MHz, $\eta = 0.7 \pm 0.1$, and $\delta_{iso} = 6 \pm 5$ ppm for site 1, and $C_Q = 3.5 \pm 0.4$ MHz, $\eta = 0.3 \pm 0.1$, and $\delta_{iso} = 6 \pm 5$ ppm for site 2 (see Table 1). Quantum chemistry calculations performed with WIEN2k with optimized crystal structures for suanite yielded $C_Q = 4.53$ and 3.56 MHz, and $\eta = 0.74$ and 0.34 for the two Mg sites, respectively.

Sinhalite, $MgAlBO_4$, crystallizes in orthorhombic space group *Pbnm*, and contains a single crystallographically unique $[MgO_6]$ site.[57] Calculated values for the ^{25}Mg NMR parameters of sinhalite are $C_Q = 5.65$ MHz, $\eta = 0.33$, and $\delta_{iso} = 7.4$ ppm (Table 1). Unfortunately, attempts at acquiring experimental ^{25}Mg NMR spectra of natural sinhalite were not successful. We suspect that elevated paramagnetic iron concentration (our mineral is brown in color, which is caused by an $O^{2-} \rightarrow Fe^{3+}$ charge transfer and Fe^{2+} in octahedral coordination in sinhalite) led to increased ^{25}Mg nuclear spin relaxation rates and a distribution of Fermi contact shifts, inhibiting ^{25}Mg NMR spectral acquisition.[64]

Grandidierite, $MgAl_3(BO_4)(SiO_4)O$, crystallizes in orthorhombic space group *Pbnm* and features one crystallographically unique Mg atom in an $[MgO_5]$ polyhedron.[60] Grandidierite has been studied previously by MacKenzie and Meinhold[7] and was one of the first crystalline compounds with a pentacoordinated Mg site to be investigated by ^{25}Mg MAS NMR spectroscopy. MacKenzie and Meinhold reported a C_Q value of 3.8 ± 0.1 MHz, an η value of 0.60 ± 0.05, and an isotropic chemical shift of 55 ± 2 ppm. The NMR parameters we obtained in this research are C_Q = 3.5 ± 0.1 MHz, η = 0.68 ± 0.15, and δ_{iso} = 23 ± 3 ppm. Note that the line width of the NMR powder pattern due to the quadrupolar interaction scales as C_Q^2/ν_0, thus the ultrahigh-field ^{25}Mg NMR spectra for grandidierite (see Figure 1c) presented in this research, acquired at B_0 = 21.1 T, possess a narrower lineshape than those previously acquired at B_0 = 11.7 T. Given the quality of our ultrahigh-field ^{25}Mg NMR spectra and the added support of calculated ^{25}Mg NMR parameters, which agree with our experimental parameters, we are confident in our newly reported ^{25}Mg NMR parameters for grandidierite.[18, 20]

Synthetic MgB_4O_7 crystallizes in orthorhombic space group *Pbca*.[2] The unit cell contains one crystallographically unique Mg site, which is coordinated by five O atoms at 1.987~2.289 Å with a mean Mg-O length of 2.094 Å.[2] The non-spinning ^{25}Mg WURST-CPMG NMR powder spectrum of MgB_4O_7, shown in Figure 2a, features clear discontinuities making NMR spectral simulation a relatively straightforward task. The ^{25}Mg NMR parameters C_Q = 10.8 ± 0.5 MHz, η = 0.35 ± 0.05, and δ_{iso} = 0 ± 30 ppm (Table 1), obtained by comparing the simulated NMR spectrum to the spikelet envelope (Figure 2a), are in good agreement with those computed using WIEN2k, C_Q = 11.31 MHz, η = 0.38, δ_{iso} = 16 ppm. Note calculated magnetic shielding parameters Ω = 25.03 ppm and κ = 0.128 (Table S2), did not detectably change the fit of the experimental simulation and therefore not included in Figure 2a.

4.1.2 Hydrous Series

The hungchaoite crystal structure in space group $P\bar{1}$ has one unique Mg site in the unit cell.[55] The Mg^{2+} cation in hungchaoite is coordinated to six oxygen atoms, five from water molecules and one that interacts with a neighboring boron atom, forming a pseudo-octahedral Mg environment. The ^{25}Mg MAS NMR spectrum for hungchaoite (Figure 1d) possesses a typical quadrupolar lineshape. The C_Q value we obtained for hungchaoite, 0.7 ± 0.1 MHz, is the smallest experimentally determined C_Q value reported herein. The asymmetry parameter for hungchaoite is $\eta = 0.8 \pm 0.2$. Quantum chemical calculations reproduced the experimental quadrupolar parameters, yielding C_Q and η values of -0.65 MHz and 0.65, respectively. The isotropic chemical shift determined from the simulation of the experimental NMR spectrum is 0.2 ± 0.5 ppm, close to our calculated value of 1.4 ppm (Table 1).

Szaibelyite crystallizes in the monoclinic space group $P2_1/a$; there are two crystallographically nonequivalent Mg^{2+} sites in the szaibelyite unit cell.[62] Mg sites 1 and 2 are coordinated to six oxygen atoms, with the local chemical environments $[MgO_5(OH)]$ and $[MgO_3(OH)_3]$, respectively. The ^{25}Mg MAS NMR spectrum (Figure 1e) features an asymmetrical lineshape with a tail to lower frequency, attributable to two overlapping NMR powder patterns corresponding to the two crystallographically nonequivalent Mg sites. Our NMR spectral simulation included two sites, with parameters $C_Q = 4.9 \pm 0.6$ MHz, $\eta = 0.75 \pm 0.05$, and $\delta_{iso} = 9 \pm 5$ ppm for site 1, and $C_Q = 3.1 \pm 0.5$ MHz, $\eta = 0.45 \pm 0.05$, and $\delta_{iso} = 12 \pm 5$ ppm for site 2 (Table 1).

The dimorphs inderite and kurnakovite crystallize in monoclinic and triclinic space groups $P2_1/c$ and $P\bar{1}$, respectively.[15, 46, 47] The Mg^{2+} cations in both inderite and kurnakovite are coordinated by six O atoms, of which four are from water molecules and the remaining two are linked to $^{[4]}B$ species [4, 5] The presence of sharp discontinuities in the ^{25}Mg MAS NMR lineshape for the dimorphs measured at 21.1 T and reported previously[26] suggests that there is a negligible

14

distribution in the bond angles and bond lengths associated with the local Mg environments.[8] Calculated C_Q and η values for inderite ($C_Q = 4.48$, $\eta = 0.4$) and kurnakovite ($C_Q = -4.78$, $\eta = 0.27$) are in agreement with our previously reported experimental C_Q and η values of 4.3 ± 0.2 MHz, 0.35 ± 0.05 and 4.5 ± 0.1 MHz, 0.30 ± 0.03 for inderite and kurnakovite, respectively (Table 1).[26]

Hydroxylborite, $Mg_3(BO_3)(OH)_3$, is the hydroxyl analogue of fluoborite[61] and is included for comparison with the latter (see below). Unfortunately, attempts to synthesize hydroxylborite for MAS NMR analysis were not successful. The calculated C_Q, η and δ_{iso} values for hydroxylborite are 3.60 MHz, 0.49 and 18.1 ppm, respectively (see Table 1).

4.1.3 Halide Series

Fluoborite, $Mg_3(BO_3)F_3$, belongs to trigonal space group $P6_3/m$ and has one crystallographically unique Mg site in the unit cell.[59] The Mg^{2+} cation in the crystal structure of fluoborite is coordinated by three fluoride anions and three oxygen atoms. The ^{25}Mg NMR parameters obtained from simulating the ^{25}Mg NMR spectrum (Figure 1f) are $C_Q = 3.85 \pm 0.20$ MHz, $\eta = 0.3 \pm 0.1$, and $\delta_{iso} = 6 \pm 3$ ppm. Calculated NMR parameters are $C_Q = 4.75$ MHz, $\eta = 0.12$ and $\delta_{iso} = 3.8$ ppm (see Table 1). The small discrepancy between the experimental and calculated C_Q values are likely caused by small random atomic site substitutions of F^- for OH^- anions beyond the initial coordination environment as hydroxyl anions often occupy F positions (*vice versa*) causing local atomic disordered within fluoborite as described by Camara and Ottolini.[59] The powder XRD data (Figure S7) are consistent with a long range structurally ordered solid, and random substitutions would be challenging to assess from our current data due to the similarity in electron density between F^- and OH^-.[65]

The boracite crystal structure in orthorhombic space group $Pca2_1$ features three crystallographically nonequivalent $[MgO_4Cl]$ polyhedra in the unit cell.[27] The boracite NMR

lineshape is broad (Figure 2b), and is expected to consist of three overlapping NMR powder patterns (Figure S8), consistent with the three crystallographically nonequivalent Mg atoms in the unit cell. The NMR spectrum does not, however, possess clear discontinuities corresponding to three unique Mg sites; note that our quantum chemical calculations indicate similar NMR parameters for all three sites (see Table 1). Nevertheless, the best fit we obtained in our NMR spectral simulation was generated using three Mg sites with experimental ^{25}Mg NMR parameter values guided by the relative magnitude of the NMR interactions predicted by our calculations. Anisotropy in chemical shift was not included in this simulation; note that the calculated spans in the magnetic shielding tensors for the three sites in boracite were approximately 20 ppm (see Table S2). A sharp, narrow resonance at ≈ 0 ppm is present in the quadrupolar echo spectrum of $Mg_3B_7O_{13}Cl$, likely attributable to a small amount of residual starting material, cubic $MgCl_2$.

$Mg_3B_7O_{13}Br$ is the bromine analogue of cubic boracite; it crystallizes in space group $F\bar{4}3c$ [66] and has one crystallographically unique six-coordinate Mg environment in the unit cell, made up of four oxygen and two bromine anions creating an extremely elongated $[MgO_4Br_2]$ tetragonal diapyramid.[9] Like MgB_4O_7, the ^{25}Mg NMR powder patterns for cubic $Mg_3B_7O_{13}Br$ are relatively broad (Figure 2c) and thus require the use of either the quadrupolar echo or WURST-CPMG pulse sequences to acquire the non-spinning ^{25}Mg NMR spectra in a reasonable time frame. The ^{25}Mg NMR lineshape for $Mg_3B_7O_{13}Br$ has well-resolved discontinuities consistent with the quadrupolar interaction. Experimental NMR parameters for $Mg_3B_7O_{13}Br$ are $C_Q = 18.0 \pm 0.3$ MHz, $\eta = 0.05 \pm 0.02$, and $\delta_{iso} = 0 \pm 30$ ppm. DFT calculations predict that the span of the chemical shift tensor is 28 ppm; including a span of *ca.* 30 ppm in our NMR spectral simulations had negligible impact on the NMR powder lineshape.

5 DISCUSSION

5.1 ^{25}Mg Nuclear Quadrupole Coupling Constants

One of the most important features of the present ultrahigh-field NMR dataset is the unusually large ^{25}Mg nuclear quadrupolar coupling constants in boracite, MgB_4O_7, and $Mg_3B_7O_{13}Br$. In particular, the C_Q value of 18.0 MHz of $Mg_3B_7O_{13}Br$, reproduced by our quantum chemical calculations, is the largest among magnesium compounds known to date.[11, 12, 16, 19] The C_Q values are sensitive to the local chemical environment at the observed nucleus as they define the interaction between the nuclear electric quadrupole moment, a physical property of an NMR-active nucleus, and the electric field gradient (EFG) tensor, which describes the change in the electric field around the nucleus.[9] If the Mg chemical environment is highly symmetric, e.g., the Mg atom occupies a regular tetrahedral or octahedral site, like in cubic MgO, the electric field gradient will be zero in each principal direction and C_Q will consequently be zero. Likewise, there will be no anisotropy in other NMR interactions. This results in a relatively sharp, narrow resonance in the NMR spectrum. In contrast, local- and medium-range deformation from spherical symmetry may result in non-zero C_Q values, broader resonances, and characteristic NMR lineshapes. Indeed, the unusually large C_Q values reported here arise from a high degree of distortion at the Mg sites. For example, the Mg sites in boracite and MgB_3O_7 have highly asymmetric pentacoordinated [MgO_4Cl] and [MgO_5] units, respectively, and the six-coordinate [MgO_4Br_2] unit in $Mg_3B_7O_{13}Br$ is an extremely elongated tetragonal dipyramid.[2, 9, 27, 28] To describe and quantify the structural information available from our experimentally observed ^{25}Mg NMR lineshapes, we look at correlations between our experimentally determined NMR parameters and a longitudinal strain parameter, adapted from the Ghose and Tsang study, which we redefine as a modified longitudinal strain, LS. LS describes the degree of distortion about Mg, and is defined as:

$$\text{LS} = \sum_{1}^{n} |r_i - r_0| / n \quad (6)$$

where r_i represents the Mg-X (X = O, F, Cl or Br) interatomic distances in the first coordination sphere, r_0 is the average interatomic distance in the Mg-X polyhedra, and n is the coordination number.[9] As is shown in Figure 3, the experimental C_Q values for all of the magnesium borates studied here correlate positively with the LS of the Mg sites. Figure S9 illustrates the relationship between either the calculated C_Q or δ_{iso} values and LS or the average Mg – O bond distance for the hydrous, anhydrous and halide-substituted magnesium borate minerals.

Interestingly, despite being originally reported as pentacoordinate,[2] the calculated δ_{iso} value for the Mg site in MgB_4O_7 is closer to the range of six-coordinate Mg sites. Bond valence sum calculations[67] show that the Mg atom in MgB_4O_7 takes only 1.753 vu with the five nearest O atoms, significantly smaller than the expected oxidation state of +2. Closer examination of the MgB_4O_7 crystal structure reveals that the Mg atom has a 6th O atom at 2.790 Å, which contributes an additional valence of 0.052 vu. Therefore, Mg in MgB_4O_7 actually adopts an unusual "5+1" coordination, and two neighboring $[MgO_6]$ polyhedra share two O atoms to form the $[Mg_2O_{10}]$ dimer. Inclusion of this coordinating oxygen shifts the LS term (Figure 3), supporting our observed experimental C_Q and isotropic chemical shift trends, *vide infra*, for a highly distorted octahedral Mg site with a revised six coordinate environment.

As C_Q and LS correlate, LS can be used to help assign ^{25}Mg sites in NMR spectra in cases of two or more nonequivalent Mg sites in the crystal structure. For example, the two crystallographically nonequivalent Mg sites[62] in szaibelyite have distinct LS parameters, corresponding to different degrees of distortion from an ideal octahedron. Thus, the C_Q values of 4.9 ± 0.6 and 3.1 ± 0.5 MHz observed experimentally are readily assigned to Mg1 and Mg2, respectively. Though this research illustrates an overall linear trend between LS and experimental or calculated C_Q values, note that the presence of different nearest-neighbor (nn) ligands (e.g.,

halides *versus* O^{2-}, $^-$OH and H_2O) may exert subtle influences on the value of C_Q. In 2009, Cahill et al.[19] hypothesized that C_Q is influenced by the nn ligands (N *vs* O), i.e., that large and small C_Q values correspond to soft and hard ligands, respectively.

Figure 4a shows that the experimental C_Q values of the magnesium borates investigated in this research are in excellent agreement with those predicted by our calculations, with a correlation coefficient, R^2, of 0.99. Note that to clearly show this correlation, all calculated C_Q values are presented as absolute values in Figure 4a; the signs of calculated C_Q values are reported in Table 1. Closer examination of Figure 4a shows that the DFT calculations underestimate the experimental results slightly for boracite and $Mg_3B_7O_{13}Br$, which possess the largest C_Q values; nevertheless the DFT calculations still predict the experimental C_Q values very well, leading to an effective predictive tool for other potentially challenging solids.

5.2 ^{25}Mg *Isotropic Chemical Shift*

The δ_{iso} values obtained from the ultrahigh-field ^{25}Mg MAS NMR spectra of the magnesium borates investigated in this research cover a range of approximately 25 ppm. This is consistent with other magnesium-containing solids with varying coordination environments,[12, 16, 19] the majority of which have δ_{iso} values between -15 and 50 ppm. DFT calculations reproduce our experimental δ_{iso} values with $R^2 = 0.93$ (see Figure 4b). Note that for the compounds with relatively large C_Q values, i.e., boracite, MgB_4O_7 and $Mg_3B_7O_{13}Br$, the limited resolution available in the WURST-CPMG NMR spectra inhibits our ability to precisely determine δ_{iso} values. Our experimental data and quantum chemistry calculations show an increase in resonance frequency with decreasing coordination number (CN), with calculated values from ~55 ppm for $[MgO_4]$, ~20 ppm for $[MgO_5]$ and <16 ppm for $[MgO_6]$. This has been observed in many other ionic solids where a lower frequency isotropic chemical shift is associated with an increase in the cation coordination

environment.[11, 68] Note that the updated experimental δ_{iso} value (above) for grandidierite, 23 ± 3 ppm, falls within the range expected for five-coordinate Mg environment.[12, 16, 19]

A plot of calculated δ_{iso} values against LS does not show a clear linear relationship (Figure S8). This suggests that though magnetic shielding is related to electronic structure, the overall geometric distortion from ideal symmetry does not govern magnetic shielding. Note that the coordination number and type of nn, e.g., water, hydroxyl, oxide or halide, impact the isotropic chemical shift. The additional effects of the nearest-neighbor H_2O and OH^- groups on the δ_{iso} values are evident by comparing the data of hungchaoite, inderite and kurnakovite with those of the anhydrous series (Table 1). The δ_{iso} values of the hydrous minerals, in which the first Mg coordination sphere contains four or five water molecules, are close to 0 ppm, the chemical shift of our reference compound, $[Mg(H_2O)_6]^{2-}$.[19] Pallister et al.[16] and Cahill et al.[19] both reported that strong hydration can lead to a decrease in resonance frequency, thus more water molecules in the first coordination sphere of Mg leads to smaller δ_{iso} values. Pallister et al. (2009)[16] interpreted such effects as the nn H_2O molecules effectively isolating the central Mg atom from shielding contributions beyond the nn. Similarly, the δ_{iso} value of the Mg2 site in szaibelyite, which has three nn OH^- groups, is 3 ppm greater than that for the Mg1 site, which has a single nn OH^- group. A similar trend has been reported for the series of Al-F minerals, where the $\delta_{iso}(^{27}Al)$ values are systematically shifted to higher frequency by > 5 ppm for Al-F minerals for each substitution of F by OH in the first coordination polyhedron of Al.[24] Such an effect is attributable to the fact that hydrogen bonding involving the OH^- group leads to a small shift to higher frequency, i.e., a deshielding effect, at the Al site.

Evaluating the shielding effects of halides for the present suite of magnesium borates is difficult, as several competitive interactions occur simultaneously. Halides in the first coordination sphere systematically shift the δ_{iso} values to lower frequency for the magnesium borates in this research.

Table 1 shows that the calculated δ_{iso} values for the [MgO$_4$Cl] polyhedra in boracite are ~12 ppm lower than that of the [MgO$_5$] polyhedron in grandidierite. Similarly, the calculated δ_{iso} value of the [MgO$_3$F$_3$] polyhedron in fluoborite is ~14 ppm less than that for the [MgO$_3$(OH)$_3$] group in hydroxylborite. In previous studies, similar effects from the substitutions of halides for O or OH have been reported in Al-F minerals[24] and zunyite;[69] this experimental observation was attributed to the more "ionic" bonding characteristics of fluorides. This trend applies to Cl and Br as well, as Mg-Cl/Br bonds are longer than Mg-O/OH bonds; the ^{25}Mg magnetic shielding is expected to decrease as substitutions are made from F to Cl and Br, displaying inverse halogen dependence.[38] In the case of boracite, the effect of the Cl atoms on the magnetic shielding can be understood in terms of strong halogen bonds, e.g., the Mg1-Cl…Mg1 and Mg2-Cl…Mg3 angles are 172° and 175°, respectively, and the Cl…Mg1 and Cl…Mg3 distances are 3.446 Å and 3.430 Å, respectively.[65, 70, 71] Finally, the trends between the δ_{iso} values and the local structural environment at Mg as well as the reverse dependence of magnetic shielding on halogens, i.e., from Br and Cl to F, observed in magnesium borates are similar to those reported for other alkaline-earth metals.[70, 72]

6 CONCLUSIONS

Ultrahigh-field ^{25}Mg NMR spectra have been acquired for a series of natural and synthetic magnesium borates at natural abundance. Simulations of the experimental ^{25}Mg NMR spectra yield quadrupolar and chemical shift NMR parameters for the Mg sites in each mineral; these values are supported by periodic *ab-initio* quantum chemistry calculations at the DFT level of theory. The experimental δ_{iso} values for these magnesium borates, which lie between 0 and 23 ppm, are within the expected range for ^{25}Mg. Experimental C_Q values quantified in this research vary from 0.7 ± 0.1 to 18.0 ± 0.3 MHz. To the best of our knowledge, the C_Q value of 18.0 ± 0.3 MHz obtained for the [MgO$_4$Br$_2$] tetragonal dipyramid in Mg$_3$B$_7$O$_{13}$Br is the largest ^{25}Mg C_Q measured by NMR reported

to date. C_Q values in this series of magnesium borates correlate positively with the modified longitudinal strain of the Mg sites. δ_{iso} values depend on the electronic environment about the magnesium nucleus, including the coordination number, but they do not correlate directly with any single structural parameter reported here. Nonetheless, our experimental C_Q and δ_{iso} parameters are reproduced accurately by our DFT calculations. These data indicate that quantum chemistry calculations are very useful as a first approach in assessing the feasibility of [25]Mg NMR experiments for magnesium borate minerals. Furthermore, MgB_4O_7 illustrates how [25]Mg NMR assists in refining poorly ambiguous coordination environments.

The data presented here are a valuable contribution to research fields involving mineralogy, geochemistry, oxide chemistry and NMR spectroscopy, and in particular are a useful addition to the literature on NMR spectroscopy of group II nuclei. As magnesium is present in many materials and minerals, we expect that the tools used in this research, i.e., NMR spectroscopy using ultrahigh magnetic field strengths, signal-enhancing pulse sequences, and accurate quantum chemistry calculations will be important in the future of materials science, geology and mineralogy research.

SUPPORTING INFORMATION

NMR acquisition parameters, powder x-ray diffraction, DFT calculated parameters, NMR simulation of Boracite-Cl and plots of calculated and experimental C_Q, δ_{iso}, LS and average bond distance.

ACKNOWLEDGEMENTS

REFERENCES:

1.   McDonough, W. F.; Sun, S.-S., The Composition of the Earth. *Chem. Geol.* **1995,** *120* (3), 223-253.

2.   Bartl, H.; Schuckmann, W., Zur Struktur Des Magnisium Diborates $MgO(B_2O_3)_2$. *N. Jb. Miner. Mh.* **1966,** *5*, 142-148.

3.   Clark, J. R.; Christ, C. L., Unusual Hydrogen Bonding in Some Hydrated Borate Structures. *Acta Cryst. B* **1977,** *33* (10), 3272-3273.

4.   Corazza, E., The Crystal Structure of Kurnakovite: A Refinement. *Acta Cryst. B* **1974,** *30* (9), 2194-2199.

5.   Corazza, E., Inderite: Crystal Structure Refinement and Relationship with Kurnakovite. *Acta Cryst. B* **1976,** *32* (5), 1329-1333.

6.   Burns, P. C.; Hawthorne, F. C.; Stirling, J. A. R., Trembathite, $(Mg,Fe)_3B_7O_{13}Cl$, a New Borate Mineral from the Salt Springs Potash Deposit, Sussex, New Brunswick. *Can. Mineral.* **1992,** *30*, 445-448.

7.   MacKenzie, K. J. D.; Meinhold, R. H., MAS NMR Study of Pentacoordinated Magnesium in Grandidierite. *Am. Mineral.* **1997,** *82*, 479-482.

8.   Zhou, B.; Michaelis, V.; Giesbrecht, S. R.; Kroeker, S.; Sherriff, B.; Sun, Z.; Yao, Y.; Pan, Y., Correlations between ^{11}B NMR Parameters and Structural Characters in Borate and Borosilicate Minerals Investigated by High-Resolution MAS NMR and Ab Initio Calculations. *Phys. Chem. Miner.* **2012,** *39* (5), 363-373.

9.   Zhou, B.; Sun, W.; Zhao, B.; Mi, J.; Laskowski, R.; Terskikh, V.; Zhang, X.; Yang, L.; Botis, S. M.; Sherriff, B. L*., et al.,* ^{11}B MAS NMR and First-Principles Study of the [OBO_3] Pyramids in Borates. *Inorg. Chem.* **2016,** *55* (5), 1970-1977.

10.   Harris, R. K.; Becker, E. D.; Cabral de Menezes, S. M.; Goodfellow, R.; Granger, P., NMR Nomenclature: Nuclear Spin Properties and Conventions for Chemical Shifts. IUPAC Recommendations 2001. International Union of Pure and Applied Chemistry. Physical Chemistry Division. Commission on Molecular Structure and Spectroscopy. *Magn. Reson. Chem.* **2002,** *40* (7), 489-505.

11.   Moudrakovski, I. L., Recent Advances in Solid-State NMR of Alkaline Earth Elements. In *Ann. Rep. NMR Spec.*, Graham, A. W., Ed. Academic Press: 2013; Volume 79, pp 129-240.

12.   Laurencin, D.; Gervais, C.; Stork, H.; Krämer, S.; Massiot, D.; Fayon, F., [25]Mg Solid-State NMR of Magnesium Phosphates: High Magnetic Field Experiments and Density Functional Theory Calculations. *J. Phys. Chem. C* **2012,** *116* (37), 19984-19995.

13. Freitas, J. C. C.; Smith, M. E., Recent Advances in Solid-State ^{25}Mg NMR Spectroscopy. *Annu. Rep. NMR Spectro.* **2012,** *75*, 25-114.

14. Kroeker, S.; Stebbins, J. F., Magnesium Coordination Environments in Glasses and Minerals: New Insight from High-Field Magnesium-25 MAS NMR. *American Mineralogist* **2000,** *85*, 1459-1464.

15. Larsen, F. H.; Jakobsen, H. J.; Ellis, P. D.; Nielsen, N. C., Sensitivity-Enhanced Quadrupolar-Echo NMR of Half-Integer Quadrupolar Nuclei. Magnitudes and Relative Orientation of Chemical Shielding and Quadrupolar Coupling Tensors. *J. Phys. Chem. A* **1997,** *101* (46), 8597-8606.

16. Pallister, P. J.; Moudrakovski, I. L.; Ripmeester, J. A., Mg-25 Ultra-High Field Solid State NMR Spectroscopy and First Principles Calculations of Magnesium Compounds. *Phys. Chem. Chem. Phys.* **2009,** *11* (48), 11487-11500.

17. Zhu, J.; Huang, Y., A Natural Abundance Solid-State ^{25}Mg NMR Study of Layered Magnesium Phosphates. *Canadian Journal of Chemistry* **2011,** *89*, 803-813.

18. Sideris, P. J.; Nielsen, U. G.; Gan, Z.; Grey, C. P., Mg/Al Ordering in Layered Double Hydroxides Revealed by Multinuclear NMR Spectroscopy. *Science* **2008,** *321* (5885), 113-117.

19. Cahill, L. S.; Hanna, J. V.; Wong, A.; Freitas, J. C. C.; Yates, J. R.; Harris, R. K.; Smith, M. E., Natural Abundance ^{25}Mg Solid-State NMR of Mg Oxyanion Systems: A Combined Experimental and Computational Study. *Chem. Eur. J.* **2009,** *15* (38), 9785-9798.

20. Ghose, S.; Tsang, T., Structural Dependence of Quadrupole Coupling Constant E^2qq/H for ^{27}Al and Crystal Field Parameter D for Fe^{3+} in Aluminosilicates. *Am. Mineral.* **1973,** *58*, 748-755.

21. Smith, M. E., Application of ^{27}Al NMR Techniques to Structure Determination in Solids. *Appl. Magn. Reson.* **1993,** *4*, 1-64.

22. Kirkpatrick, R. J.; Phillips, B. L., ^{27}Al NMR Spectroscopy of Minerals and Related Materials. *Appl. Magn. Reson.* **1993,** *4* (1), 213-236.

23. MacKenzie, K. J. D.; Smith, M. E., *Multinuclear Solid-State NMR of Inorganic Materials*. Pergamon: Amsterdam, 2002.

24. Zhou, B.; Sherriff, B. L.; Hartman, J. S.; Wu, G., ^{27}Al and ^{23}Na NMR Spectroscopy and Structural Modeling of Aluminofluoride Minerals. *Am. Mineral.* **2007,** *92* (1), 34-43.

25. Michaelis, V. K.; Kroeker, S., ^{73}Ge Solid-State NMR of Germanium Oxide Materials: Experimental and Theoretical Studies. *J. Phys. Chem. C* **2010,** *114* (49), 21736-21744.

26. Zhou, B.; Michaelis, V. K.; Pan, Y.; Yao, Y.; Tait, K. T.; Hyde, B. C.; Wren, J. E. C.; Sherriff, B. L.; Kroeker, S., Crystal Structure Refinements of Borate Dimorphs Inderite and

Kurnakovite Using [11]B and [25]Mg Nuclear Magnetic Resonance and Dft Calculations. *Am. Mineral.* **2012,** *97* (11-12), 1858-1865.

27.   Dowty, E.; Clark, J. R., Crystal-Structure Refinements for Orthorhombic Boracite, $Mg_3ClB_7O_{13}$, and a Trigonal, Iron-Rich Analogue. *Z. Kristallog.* **1973,** *Bd.138* (1-6), 64-99.

28.   Oliveira, T. M.; Lima, A. F.; Brik, M. G.; Souza, S. O.; Lalic, M. V., Electronic Structure and Optical Properties of Magnesium Tetraborate: An Ab Initio Study. *Comput. Mater. Sci.* **2016,** *124*, 1-7.

29.   Slichter, C. P., *Principles of Magnetic Resonance*. Springer Verlag, Berlin, Heidelberg, New York, 1992.

30.   Man, P. P., Quadrupolar Interactions. In *Emagres*, John Wiley & Sons, Ltd: 2007.

31.   Wasylishen, R. E.; Ashbrook, S. E.; Wimperis, S., *NMR of Quadrupolar Nuclei in Solid Materials*. John Wiley & Sons Ltd.: Chichester, UK, 2012.

32.   Herzfeld, J.; Berger, A. E., Sideband Intensitites in NMR-Spectra of Samples Spinning at the Magic Angle. *J. Chem. Phys.* **1980,** *73* (12), 6021−6030.

33.   Mason, J., Conventions for the Reporting of Nuclear Magnetic Shielding (or Shift) Tensors Suggested by Participants in the NATO ARW on NMR Shielding Constants at the University of Maryland, College Park, July 1992. *Solid State Nucl. Magn. Reson.* **1993,** *2* (5), 285-288.

34.   Charpentier, T., The PAW/GIPAW Approach for Computing NMR Parameters: A New Dimension Added to NMR Study of Solids. *Solid State Nucl. Magn. Reson.* **2011,** *40* (1), 1-20.

35.   Bonhomme, C.; Gervais, C.; Babonneau, F.; Coelho, C.; Pourpoint, F.; Azaïs, T.; Ashbrook, S. E.; Griffin, J. M.; Yates, J. R.; Mauri, F.*, et al.*, First-Principles Calculation of NMR Parameters Using the Gauge Including Projector Augmented Wave Method: A Chemist's Point of View. *Chem. Rev.* **2012,** *112* (11), 5733-5779.

36.   Clark, S. J.; Segall, M. D.; Pickard, C. J.; Hasnip, P. J.; Probert, M. I. J.; Refson, K.; Payne, M. C., First Principles Methods Using Castep. *Z. Kristallogr. - Cryst. Mater.* **2005,** *220*, 567−570.

37.   Pickard, C. J.; Mauri, F., All-Electron Magnetic Response with Pseudopotentials: NMR Chemical Shifts. *Phys. Rev. B: Condens. Matter Mater. Phys.* **2001,** *63* (24), 245101.

38.   Yates, J. R.; Pickard, C. J.; Mauri, F., Calculation of NMR Chemical Shifts for Extended Systems Using Ultrasoft Pseudopotentials. *Phys. Rev. B: Condens. Matter Mater. Phys.* **2007,** *76* (2), 024401.

39.   Laskowski, R.; Blaha, P., Origin of NMR Shielding in Fluorides. *Phys. Rev. B* **2012,** *85* (24), 245117.

40.   Laskowski, R.; Blaha, P., Calculations of NMR Chemical Shifts with APW-Based Methods. *Phys. Rev. B* **2012,** *85* (3), 035132.

41.   Laskowski, R.; Blaha, P., Understanding of [33]S NMR Shielding in Inorganic Sulfides and Sulfates. *J. Phys. Chem. C* **2015,** *119* (1), 731-740.

42.   Laskowski, R.; Blaha, P.; Tran, F., Assessment of DFT Functionals with NMR Chemical Shifts. *Phys. Rev. B* **2013,** *87* (19), 195130.

43.   Laskowski, R.; Khoo, K. H.; Haarmann, F.; Blaha, P., Computational Study of Ga NMR Shielding in Metallic Gallides. *The Journal of Physical Chemistry C* **2017,** *121* (1), 753-760.

44.   Blaha, P.; Schwarz, K.; Herzig, P., First-Principles Calculation of the Electric Field Gradient of Li_3N. *Phys. Rev. Lett.* **1985,** *54* (11), 1192-1195.

45.   Blaha, P.; Schwarz, K.; Dederichs, P. H., First-Principles Calculation of the Electric-Field Gradient in HCP Metals. *Phys. Rev. B* **1988,** *37* (6), 2792-2796.

46.   Blaha, P.; Schwarz, K.; Sorantin, P.; Trickey, S. B., Full-Potential, Linearized Augmented Plane Wave Programs for Crystalline Systems. *Comput. Phys. Commun.* **1990,** *59* (2), 399-415.

47.   Blaha, P.; Singh, D. J.; Sorantin, P. I.; Schwarz, K., Electric-Field-Gradient Calculations for Systems with Large Extended-Core-State Contributions. *Phys. Rev. B* **1992,** *46* (3), 1321-1325.

48.   Blaha, P.; Schwarz, K.; Madsen, G. K.; Kvasnicka, D.; Luitz, J., *Wien2k, an Augmented Plane Wave+Local Orbitals Program for Calculating Crystal Properties.* Karlheinz Schwarz, TechnischeUniversität Wien, Vienna, 2001.

49.   Zhou, B.; Michaelis, V. K.; Kroeker, S.; Wren, J. E. C.; Yao, Y.; Sherriff, B. L.; Pan, Y., ^{11}B and ^{23}Na Solid-State NMR and Density Functional Theory Studies of Electric Field Gradients at Boron Sites in Ulexite. *Cryst. Eng. Comm.* **2013,** *15* (43), 8739-8747.

50.   Zhou, B.; Michaelis, V. K.; Yao, Y.; Sherriff, B. L.; Kroeker, S.; Pan, Y., Density Functional Theory Study of the Magnetic Shielding Mechanism for [11]B in Pentaborate Minerals: Ulexite and Probertite. *Cryst. Eng. Comm.* **2014,** *16* (45), 10418-10427.

51.   Schurko, R. W., Ultra-Wideline Solid-State NMR Spectroscopy. *Acc. Chem. Res.* **2013,** *46* (9), 1985-1995.

52.   O'Dell, L. A.; Rossini, A. J.; Schurko, R. W., Acquisition of Ultra-Wideline NMR Spectra from Quadrupolar Nuclei by Frequency Stepped WURST–QCPMG. *Chemical Physics Letters* **2009,** *468* (4–6), 330-335.

53.   Eichele, K.; Wasylishen, R. E., Wsolids NMR Simulation Package, Version 1.17.26. **2000**.

54.   Torumba, D.; Parlinski, K.; Rots, M.; Cottenier, S., Temperature Dependence of the Electric-Field Gradient in HCP-Cd from First Principles. *Phys. Rev. B* **2006,** *74* (14), 144304.

55.   Wan, C.; Ghose, S., Hungchaoite, $Mg(H_2O)_5B_4O_5(OH)_4 \cdot 2H_2O$: A Hydrogen-Bonded Molecular Complex. *Am. Mineral.* **1977,** *62* (11-12), 1135-1143.

56.   Effenberger, H.; Pertlik, F., Verfeinerung Der Kristallstrukturen Der Isotypen Verbindungen $M_3(BO_3)_2$ Mit M = Mg, Co Und Ni (Strukturtyp: Kotoit). *Z. Kristallog.* **1984,** *166* (1-4), 129-140.

57.   Hayward, C.; Angel, R. J.; Ross, N. L., The Structural Redetermination and Crystal Chemistry of Sinhalite, $MgAlBO_4$. *Eur. J. Mineral.* **1994,** *6* (3), 313-321.

58.   Guo, G. C.; Cheng, W. D.; Chen, J. T.; Zhuang, H. H.; Huang, J. S.; Zhang, Q. E., Monoclinic $Mg_2B_2O_5$. *Acta Cryst. C* **1995,** *51* (12), 2469-2471.

59.   Cámara, F.; Ottolini, L., New Data on the Crystal-Chemistry of Fluoborite by Means of SREF, SIMS, and EMP Analysis. *Am. Mineral.* **2000,** *85* (1), 103-107.

60.   Dzikowski, T. J.; Groat, L. A.; Grew, E. S., The Geometric Effects of VFe^{2+} for Vmg Substitution on the Crystal Structures of the Grandidierite-Ominelite Series. *Am. Mineral.* **2007,** *92* (5-6), 863-872.

61.   Rudnev, V. V.; Chukanov, N. V.; Nechelyustov, G. N.; Yamnova, N. A., Hydroxylborite, $Mg_3(BO_3)(OH)_3$, a New Mineral Species and Isomorphous Series Fluoborite-Hydroxylborite. *Geol. Ore Deposits* **2007,** *49* (8), 710-719.

62.   Grice, J. D., Szaibélyite: Crystal-Structure Analysis and Hydrogen Bonding. *Can. Mineral.* **2008,** *46* (3), 671-677.

63.   Dupree, R.; Smith, M. E., Solid-State Magnesium-25 N.M.R. Spectroscopy. *J. Chem. Soc., Chem. Commun.* **1988,** (22), 1483-1485.

64.   Lottermoser, W.; Redhammer, G. J.; Weber, S.-U.; Litterst, F. J.; Tippelt, G.; Dlugosz, S.; Bank, H.; Amthauer, G.; Grodzicki, M., The Electric Field Gradient in Natural Iron-Doped Chrysoberyl Al_2BeO_4 and Sinhalite Mgalbo$_4$ Single Crystals. *Phys. Chem. Minerals* **2011,** *38* (10), 787-799.

65.   Mi, J.-X.; Pan, Y., *Halogen-Rich Minerals: Crystal Chemistry and Geological Significances. In "Role of Halogens in Terrestrial and Extraterrestrial Processes"*. Harlov, D. ed.,Springer (accepted): 2017.

66.   Sueno, S.; Clark, J. R.; Papike, J. J.; Konnert, J. A., Crystal Structure Refinement of Cubic Boracite. *Am. Mineral.* **1973,** *58*, 691-697.

67.   Brown, I. D., Recent Developments in the Methods and Applications of the Bond Valence Model. *Chem. Rev.* **2009,** *109* (12), 6858-6919.

68.   Michaelis, V. K.; Aguiar, P. M.; Kroeker, S., Probing Alkali Coordination Environments in Alkali Borate Glasses by Multinuclear Magnetic Resonance. *J. Non-Crystal Solids* **2007,** *353* (26), 2582-2590.

69.   Zhou, B.; Sherriff, B. L.; Taulelle, F.; Wu, G., Nuclear Magnetic Resonance Study of Al:Si and F:OH Order in Zunyite. *Can. Mineral.* **2003,** *41* (4), 891-903.

70.   Burgess, K. M. N.; Xu, Y.; Leclerc, M. C.; Bryce, D. L., Alkaline-Earth Metal Carboxylates Characterized by [43]Ca and [87]Sr Solid-State NMR: Impact of Metal-Amine Bonding. *Inorg. Chem.* **2014,** *53* (1), 552-561.

71.   Cavallo, G.; Metrangolo, P.; Milani, R.; Pilati, T.; Priimagi, A.; Resnati, G.; Terraneo, G., The Halogen Bond. *Chem. Rev.* **2016,** *116* (4), 2478-2601.

72.   Faucher, A.; Terskikh, V. V.; Ye, E.; Bernard, G. M.; Wasylishen, R. E., Solid-State [87]Sr NMR Spectroscopy at Natural Abundance and High Magnetic Field Strength. *J. Phys. Chem. A* **2015,** *119* (49), 11847-11861.
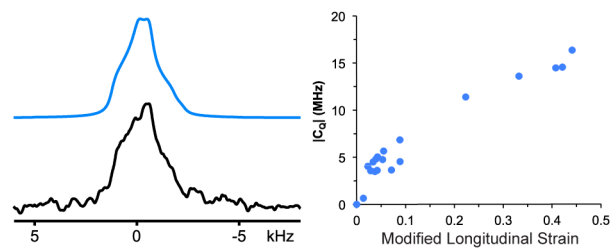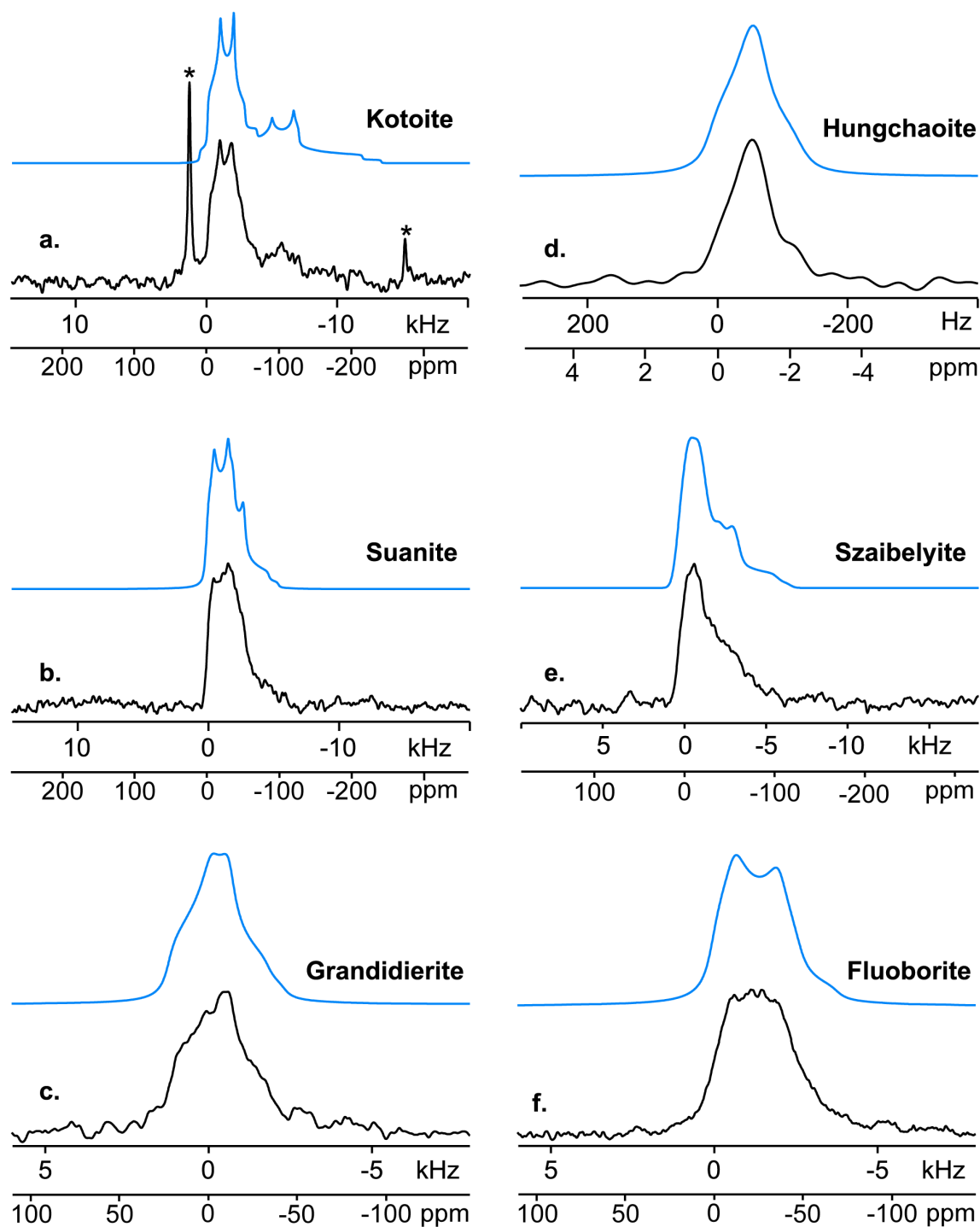
Figures
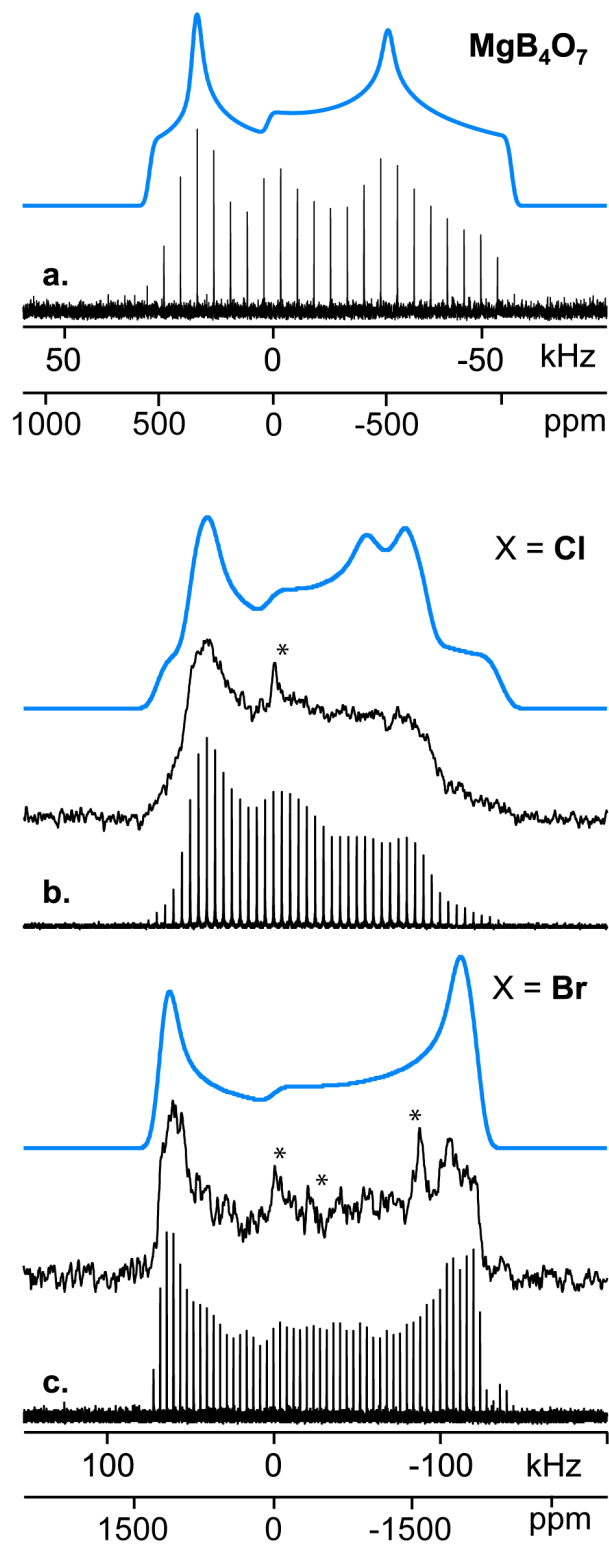

**Figure 1.** Experimental (lower traces, black) and simulated (upper traces, blue) ^{25}Mg MAS NMR spectra of (a) kotoite, $Mg_3B_2O_6$; (b) suanite, $Mg_2B_2O_5$, (c) grandidierite, $MgAl_3(BO_4)(SiO_4)O$, (d) hungchaoite, $MgB_4O_5(OH)_4 \cdot 3(H_2O)$, (e) szaibelyite, $MgBO_2(OH)$, and (f) fluoborite, $Mg_3(BO_3)(F,OH)_3$. Experimental NMR spectra were acquired at $B_0 = 21.1$ T. Asterisks (*) indicate NMR peaks from MgO. Simulated NMR spectra were generated with WSolids using the NMR parameters listed in Table 1.

Figure 2. Experimental (lower traces, black) and simulated (upper traces, blue) ^{25}Mg NMR spectra of stationary (a) MgB_4O_7, and (b and c) boracite-type compounds, $Mg_3B_7O_{13}X$ (X = Cl, Br). Experimental NMR spectra acquired at $B_0 =$ 21.1 T. Simulated NMR spectra were generated with WSolids using the NMR parameters listed in Table 1. *Intensities are due to a small number of larger crystals within the powder samples.
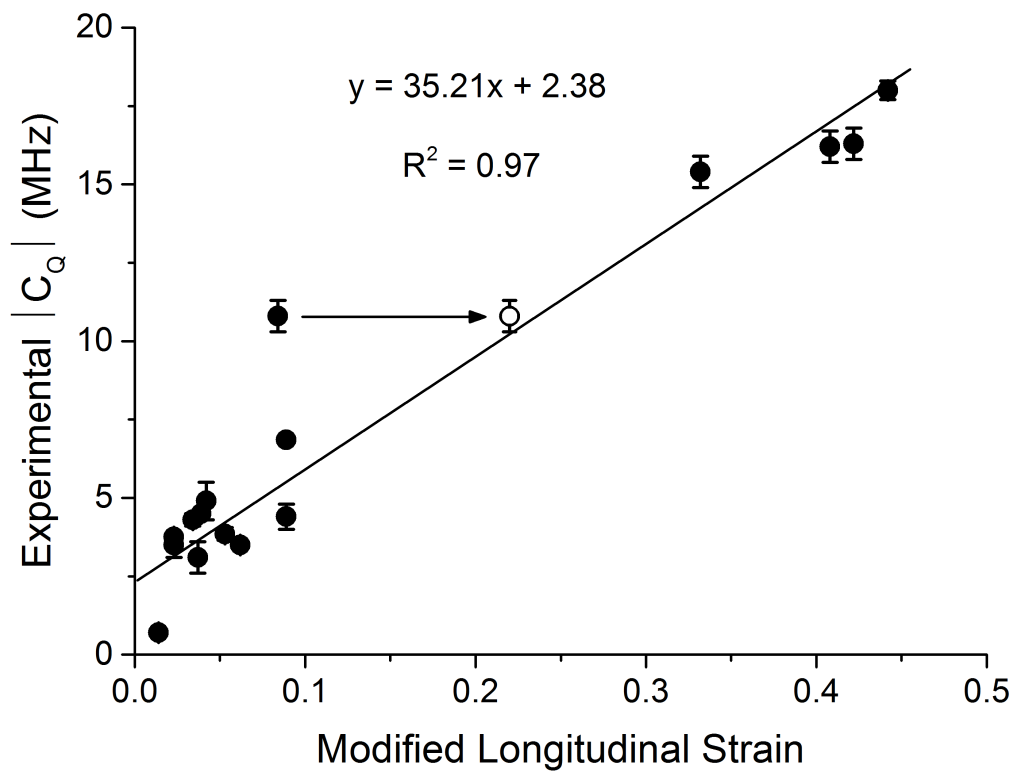
Figure 3: Correlation between experimental $|C_Q|$ values and the modified longitudinal strain. The correlation coefficient is $R^2 = 0.97$ with adjustment for a six-coordinate Mg site in MgB_4O_7 (open circle, see text for explanation).
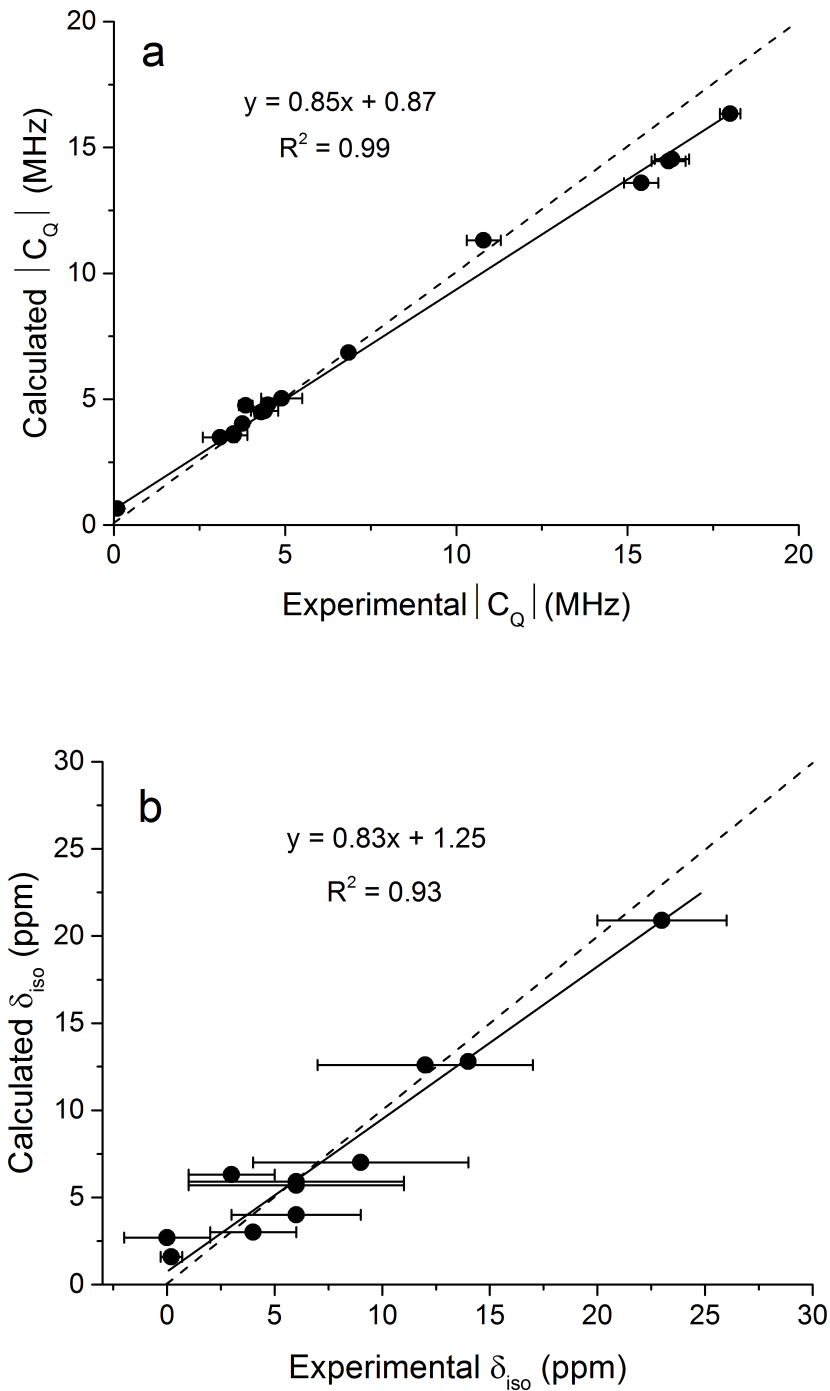
Figure 4. Correlation between (a) calculated and experimental $|C_Q|$ values and (b) calculated and experimental isotropic chemical shift values. Calculated [25]Mg NMR parameters were obtained using the WIEN2k program package. Note that the experimental δ_{iso} values for boracite, MgB_4O_7 and $Mg_3B_7O_{13}Br$ are associated with large uncertainties and therefore not included in (b). The black dotted lines indicate a 1:1 relationship between the experimental and calculated NMR parameters.

Table 1. ^{25}Mg experimental and DFT calculated NMR parameters

Formula	Mineral Name	Mgφ_x	LS	Experimental			Calculated			
				$|C_Q|$ (MHz)	η	δ_{iso} (ppm)	C_Q (MHz)	η	σ_{iso} (ppm)	δ_{iso} (ppm)[d]
Anhydrous Series										
Mg$_3$B$_2$O$_6$	kotoite	Mg1O$_6$	0.089	6.85[b]	0.76[b]	14[b]	−6.85	0.76	551.9	12.6
		Mg2O$_6$	0.023	3.75 (10)	0.45(5)	4(2)	4.03	0.46	561.7	2.8
Mg$_2$B$_2$O$_5$	suanite	Mg1O$_6$	0.089	4.4(4)	0.7(1)	6(5)	4.53	0.74	558.8	5.7
		Mg2O$_6$	0.023	3.5(4)	0.3(1)	6(5)	3.56	0.34	559.0	5.5
MgAlBO$_4$	sinhalite	MgO$_6$	0.055	nd	nd	nd	5.65	0.33	557.1	7.4
MgAl$_3$BSiO$_9$	grandidierite	MgO$_5$	0.004	3.5(1)	0.68(15)	23(3)	3.64	0.68	543.8	20.7
MgB$_4$O$_7$		MgO$_5$ / MgO$_6$*	0.084/0.220*	10.8(5)	0.35(5)	0(30)	11.31	0.38	548.7	15.8
Hydrous Series										
MgBO$_2$(OH)	szaibelyite	Mg1O$_5$(OH)	0.042	4.9(6)	0.75(5)	9(5)	−5.03	0.91	557.7	6.8
		Mg2O$_3$(OH)$_3$	0.037	3.1(5)	0.45(5)	12(5)	−3.48	0.48	552.1	12.4
MgB$_4$O$_5$(OH)$_4$·3H$_2$O	hungchaoite	Mg(OH)(H$_2$O)$_5$	0.014	0.7(1)	0.8(2)	0.2(5)	−0.65	0.65	563.1	1.4
MgB$_3$O$_3$(OH)$_5$·5H$_2$O	inderite[a]	MgO$_2$(H$_2$O)$_4$	0.034	4.3(2)	0.35(5)	0(2)	4.48	0.40	562.0	2.5
MgB$_3$O$_3$(OH)$_5$·5H$_2$O	kurnakovite[a]	MgO(H$_2$O)$_5$	0.039	4.5(1)	0.30(3)	3(2)	−4.78	0.27	558.4	6.1
Mg$_3$(BO$_3$)(OH)$_3$	hydroxylborite	MgO$_3$(OH)$_3$	0.042	nd	nd	nd	3.60	0.49	546.6	17.1
Halide Series										
Mg$_3$(BO$_3$)F$_3$	fluoborite	MgO$_3$F$_3$	0.053	3.85(20)	0.3(1)	6(3)	4.75	0.12	560.7	3.8
Mg$_3$B$_7$O$_{13}$Br		MgO$_4$Br$_2$	0.442	18.0(3)	0.05(2)	0(30)	16.34	0.00	554.8	9.7
Mg$_3$B$_7$O$_{13}$Cl	boracite	Mg1O$_4$Cl	0.332	15.4(5)	0.08(10)	0(30)	13.59	0.06	555.7	8.8
		Mg2O$_4$Cl	0.408	16.2(5)	0.4(1)	0(30)	14.46	0.46	555.9	8.6
		Mg3O$_4$Cl	0.422	16.3(5)	0.45(10)	0(30)	14.54	0.54	554.3	10.2
Reference Compounds										
MgO	periclase[f]	MgO$_6$	0	0	0	0	26(1)	0	0	535.0	29.5
Mg(OH)$_2$	brucite[c]	Mg(OH)$_6$	0.002	3.09(1)	0.00(1)	11.8(2)	2.10	0.42	550.8	13.7
MgAl$_2$O$_4$	spinel[c]	MgO$_4$	0	0.00	nd	48(1)	0.000	0.00	509.3	55.2

[a] Experimental data from Zhou et al., *Am. Mineral.*, **2012**, *97*, 1858-1865.

*The LS values for MgB$_4$O$_7$ for five- and six-coordinate Mg, respectively (see text for explanation).

[b] NMR parameters used in spectral simulation were determined via DFT calculations.

[c] NMR experimental data for brucite and spinel are from Pallister et al., *Phys. Chem. Chem. Phys.*, **2009**, *11*, 11487–11500.

[d] $\delta_{iso} = -(\sigma_{iso} - 564.5 \text{ ppm})$

[f] NMR experimental data for periclase are from Dupree and Smith, *J. Chem. Soc. Chem. Comm.*, **1988**, 1483-1485.

φ_x: denoting the nearest-neighbors such as O, OH, H$_2$O, F, Cl or Br.

nd: not determined.

LS: modified longitudinal strain (see text for definition).